Ⅳ. 研究成果の刊行物・別冊

Short Report

Molecular Syndromology

Mol Syndromol 2015;6:50–53
DOI: 10.1159/000370337

Accepted: May 8, 2014
by M. Schmid
Published online: January 29, 2015

A Glutamine Repeat Variant of the *RUNX2* Gene Causes Cleidocranial Dysplasia

Masaki Mastushita[a] Hiroshi Kitoh[a] Asli Subasioglu[b] Fatma Kurt Colak[c]
Munis Dundar[c] Kenichi Mishima[a] Yoshihiro Nishida[a] Naoki Ishiguro[a]

[a]Department of Orthopedic Surgery, Nagoya University Graduate School of Medicine, Nagoya, Japan;
[b]Department of Medical Genetics, Izmir Katip Celebi University Ataturk Training and Research Hospital, Izmir, and
[c]Department of Medical Genetics, Erciyes University, Kayseri, Turkey

Key Words
Cleidocranial dysplasia · Glutamine repeat variant · Q/A domain · *RUNX2*

Abstract
Cleidocranial dysplasia (CCD), an autosomal dominant skeletal dysplasia characterized by hypoplastic clavicles and delayed closure of the cranial sutures, is caused by mutations of the runt-related transcription factor 2 *(RUNX2)* gene. The *RUNX2* gene consists of a glutamine and alanine repeat domain (Q/A domain, 23Q/17A), a DNA-binding Runt domain and a proline/serine/threonine-rich domain. We report on a familial case of CCD with a novel mutation within the Q/A domain of the *RUNX2* gene, which is an insertion in exon 1 (p.Q71_E72insQQQQ) representing the Q-repeat variant (27Q/17A). Functional analysis of the 27Q variant revealed abolished transactivation capacity of the mutated RUNX2 protein. This is the first case report that demonstrated a glutamine repeat variant of the *RUNX2* gene causes CCD.

Cleidocranial dysplasia (CCD) is an autosomal dominant skeletal dysplasia characterized by hypoplastic or aplastic clavicles, delayed closure of the fontanelles and cranial sutures, delayed ossification of the pelvis, dental abnormalities such as late eruption of permanent teeth and multiple supernumerary teeth, and moderately short stature [Cooper et al., 2001]. CCD is caused by hypomorphic or haploinsufficiency of the runt-related transcription factor 2 *(RUNX2)* gene [Lee et al., 1997; Mundlos et al., 1997].

To date, the mutations occur throughout the *RUNX2* gene, but are clustered in the Runt domain in CCD. Most of the mutations within the Runt domain are missense mutations. On the other hand, nonsense mutations, insertions or deletions are predominant within the Q/A domain or the proline/serine/threonine-rich domain [Kim et al., 2006]. The Q/A domain has the capacity to mutate via strand slippage during DNA replication [Yoshida et al., 2002]. Glutamine repeat sequence expansion has been the cause of some diseases that show genetic anticipation, where severity increases in subsequent generations as the repeat length increases due to errors in replication [McMurray, 2010]. Wild-type human *RUNX2* contains a

1661–8769/15/0061–0050$39.50/0

E-Mail karger@karger.com
www.karger.com/msy

Hiroshi Kitoh, MD
Department of Orthopedic Surgery
Nagoya University Graduate School of Medicine
65 Tsurumai-cho, Showa-ku, Nagoya 466-8550 (Japan)
E-Mail hkitoh@med.nagoya-u.ac.jp

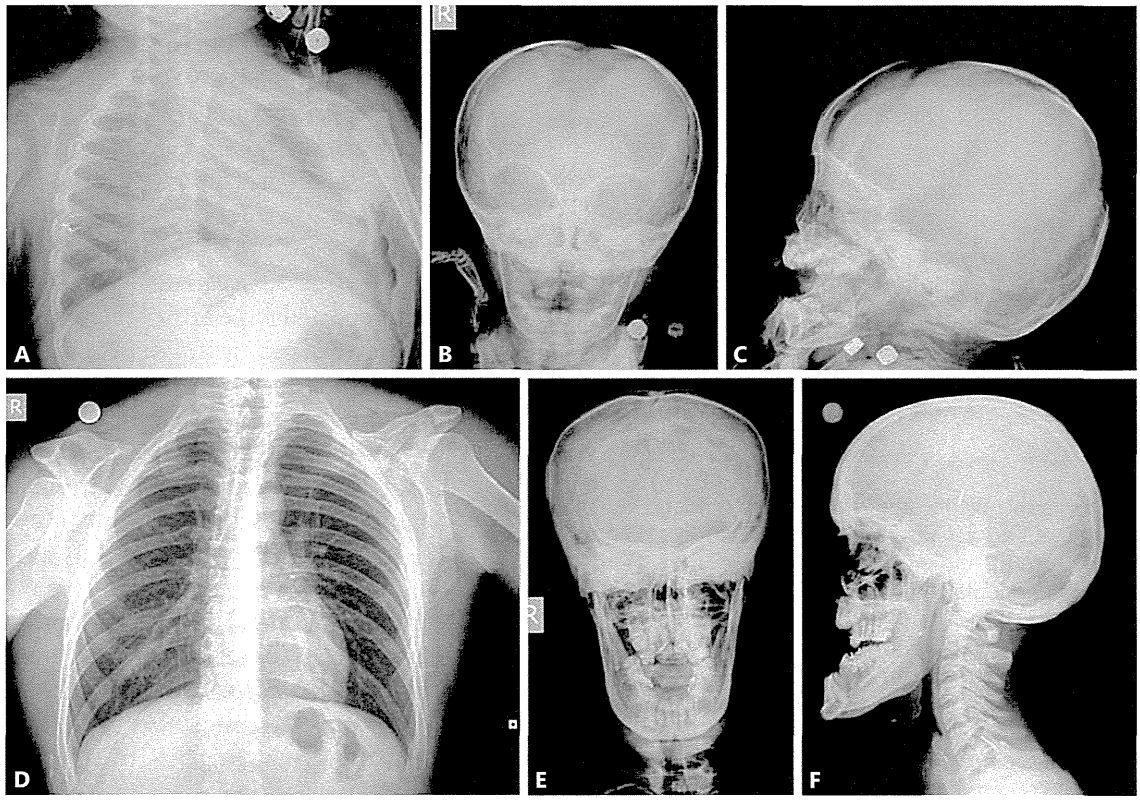

Fig. 1. Radiographs of the proband's chest and skull demonstrating the complete absence of bilateral clavicles, open large fontanelles, multiple wormian bones, supernumerary teeth, and mandibular protrusion (**A–C**). Anteroposterior radiograph of the father's chest demonstrating bilateral absence of clavicles (**D**) and radiographs of his skull demonstrating multiple wormian bones, a relatively thick skull and prognathism (**E**, **F**).

23Q/17A repeat: 23 consecutive glutamine residues followed by 17 alanine residues. An insertion of the polyalanine tract (23Q/27A) was previously observed in only one CCD patient [Mundlos et al., 1997].

Here, we describe a familial case of CCD with a novel mutation within the Q/A domain, which is an insertion of the polyglutamine tract (27Q/17A). In vitro functional analysis was performed to assay the transactivation capacity of the mutant RUNX2 protein.

Case Report

A family with the clinical diagnosis of CCD from the Erciyes University, Turkey, was examined in this study. The proband, a 2-year-old boy, is the only child of an affected father (27 years old) and a healthy mother (23 years old). Radiographs of the proband showed a large defect of the parietal and occipital bones, supernumerary teeth, sclerosis of the cranial base, multiple wormian bones, and bilateral absence of clavicles (fig. 1A–C). The last 2 radiographic manifestations (multiple wormian bones and absent clavicles) were also observed in the boy's father (fig. 1D, E), although he had a relatively thick skull and prognathism (fig. 1F). The craniofacial manifestations, including frontal bossing, midface hypoplasia and a small face, were shared in both the proband and his father.

Methods

After informed consent was obtained from all family members, genomic DNA was extracted from peripheral blood leukocytes. The exons (0–7) and their flanking intronic regions of the *RUNX2* gene were amplified by PCR using sets of primers. Direct sequence analysis of the affected patients' DNA from this family demonstrated a novel heterozygous mutation within the Q/A domain, c.213_214insCAGCAGCAGCAG (p.Q71_E72insQQQQ).

For in vitro functional studies of the mutant RUNX2 protein identified in this family, the entire cDNA of p.Q71_E72insQQQQ (27Q) was constructed as follows. We confirmed that the mutation was located between 2 PstI sites (181 bp) in exon 1 and obtained the oligonucleotide duplex containing the mutation (Integrated

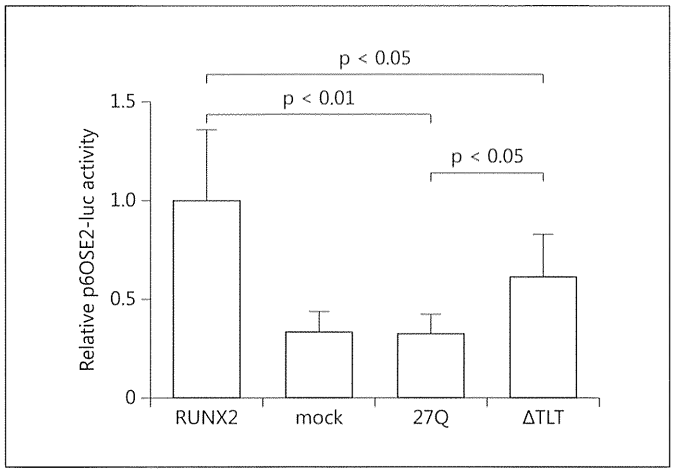

Fig. 2. Transactivation ability of the wild-type and mutant RUNX2 proteins. COS7 cells were transfected with p6OSE2-luc as a reporter plasmid, full-length, wild-type or mutant RUNX2 as effector plasmids, and phRL-TK as an internal control of transfection efficiency. Data are presented as fold activation relative to the activity obtained with wild-type RUNX2 vector plasmid. Bars represent the average ratios of luciferase to Renilla activity. Standard deviations are represented by error bars. Both the 27Q variant and ΔTLT198_200 mutants showed significantly reduced transactivation ability compared to the wild type. Moreover, transactivation of the 27Q variant was significantly lower than that of the ΔTLT198_200 mutant.

DNA Technologies MBL, Japan). PCR fragments of the oligonucleotide duplex were double-digested with PstI. This insert was cloned into the human full-length *RUNX2* cDNA (Ori-Gene Technologies, Rockville, Md., USA) at the PstI sites. On the other hand, p.T198_T200del (ΔTLT), which was previously identified in a patient with CCD, was constructed by using the QuikChange site-directed mutagenesis kit (Stratagene, La Jolla, Calif., USA) [Matsushita et al., 2014]. Transient transfection experiments in COS7 cells were performed using FuGENE 6 (Roche, Indianapolis, Ind., USA). Aliquots of 400 ng expression plasmid containing either wild-type or mutagenized *RUNX2* were cotransfected with 400 ng of a reporter plasmid p6OSE2-luc (kindly provided by T. Komori, Nagasaki University, Japan) [Harada et al., 1999]. All transfection experiments were done 8 times. The transactivation study showed that the 27Q variant and ΔTLT mutants had significantly lower transcription activities (32 and 61% of the wild type, respectively) (fig. 2).

Discussion

Clinical and radiographic manifestations of the present cases seemed to be typical for CCD, including complete absence of bilateral clavicles, multiple wormian bones and supernumerary teeth. Mutation analysis of this family showed a Q-repeat variant within the Q/A domain, which resulted in a significant reduction of transactivation of the RUNX2 protein.

Q-repeat variants within the *RUNX2* gene were identified in an Australian fracture cohort (15Q, 16Q, 24Q, and 30Q) [Vaughan et al., 2002], a randomly selected population from Aberdeen (16Q) [Vaughan et al., 2004], and a Spanish population study (16Q, 18Q and 30Q) [Pineda et al., 2010]. A 30Q variant of the *RUNX2* gene has never been reported to be associated with CCD phenotypes. On the other hand, a novel 27Q variant caused CCD by downregulating the transactivation activity of the RUNX2 protein. Generally, triplet repeat expansion disorders accelerate their phenotypes according to the repeat length. Huntington's disease, for example, is one of the polyQ-repeat disorders, and its severity is usually associated with the length of the polyQ tracts. It has been suggested that aggregation of the polyQ fibers is pathogenic of the disease. Perutz [1996] reported that Huntington's disease has not been observed in individuals with <37 repeats, and absence of disease has never been found in those with >41 repeats. This indicated that polyQ expansion beyond the pathological threshold of 36–40 repeats leads to a clinical manifestation. According to the model of Perutz et al. [2002], polyQ fibers are composed of nanotubes with 20 residues per turn, and a minimum of 2 turns (40 repeats) is necessary for pathogenic polyQ aggregates. It is possible that the 27Q variant is pathogenic, while the 30Q variant is benign, since the repeat length is not necessarily related to the severity of the disease when it is <40 repeats.

Sears et al. [2007] showed that Q/A tandem repeat ratio correlated to *RUNX2* transcriptional activity. Morrison et al. [2012] demonstrated that transactivation activity was reduced by the *RUNX2* Q-repeat variants, but rescued by PEBP2β, which is the partner subunit for heterodimerization with the Runt domain. In a study on dogs, Fondon and Garner [2004] demonstrated that the length of the Q repeat is significantly associated with midface length and nose curvature. We previously reported a CCD patient with the in-frame deletion (ΔTLT) who showed a milder phenotype than the present cases, including mild short stature (–1.75 SD), delayed fontanelle, midface hypoplasia, pseudoarthrosis of the right clavicle, and hypoplasia of the left clavicle [Matsushita et al., 2014]. ΔTLT mutation decreased the transactivation activity of the RUNX2 protein by abolishing the heterodimerization of the RUNX2 protein with the PEBP2β. Significantly lower transactivation activity of the 27Q variant than that of the ΔTLT mutant may reflect the phenotypic severity of the disease.

References

Cooper SC, Flaitz CM, Johnston DA, Lee B, Hecht JT: A natural history of cleidocranial dysplasia. Am J Med Genet 104:1–6 (2001).

Fondon JW 3rd, Garner HR: Molecular origins of rapid and continuous morphological evolution. Proc Natl Acad Sci USA 101:18058–18063 (2004).

Harada H, Tagashira S, Fujiwara M, Ogawa S, Katsumata T, et al: *Cbfa1* isoforms exert functional differences in osteoblast differentiation. J Biol Chem 274:6972–6978 (1999).

Kim HJ, Nam SH, Kim HJ, Park HS, Ryoo HM, et al: Four novel *RUNX2* mutations including a splice donor site result in the cleidocranial dysplasia phenotype. J Cell Physiol 207:114–122 (2006).

Lee B, Thirunavukkarasu K, Zhou L, Pastore L, Baldini A, et al: Missense mutations abolishing DNA binding of the osteoblast-specific transcription factor OSF2/CBFA1 in cleidocranial dysplasia. Nat Genet 16:307–310 (1997).

Matsushita M, Kitoh H, Kaneko H, Mishima K, Itoh Y, et al: A novel in-frame deletion of the *RUNX2* gene causes a classic form of cleidocranial dysplasia. J Bone Miner Metab 32:96–99 (2014).

McMurray CT: Mechanisms of trinucleotide repeat instability during human development. Nat Rev Genet 11:786–799 (2010).

Morrison NA, Stephens AA, Osato M, Polly P, Tan TC, et al: Glutamine repeat variants in human RUNX2 associated with decreased femoral neck BMD, broadband ultrasound attenuation and target gene transactivation. PLoS One 7:e42617 (2012).

Mundlos S, Otto F, Mundlos C, Mulliken JB, Aylsworth AS, et al: Mutations involving the transcription factor CBFA1 cause cleidocranial dysplasia. Cell 89:773–779 (1997).

Perutz MF: Glutamine repeats and inherited neurodegenerative diseases: molecular aspects. Curr Opin Struct Biol 6:848–858 (1996).

Perutz MF, Finch JT, Berriman J, Lesk A: Amyloid fibers are water-filled nanotubes. Proc Natl Acad Sci USA 99:5591–5595 (2002).

Pineda B, Hermenegildo C, Laporta P, Tarín JJ, Cano A, García-Pérez MÁ: Common polymorphisms rather than rare genetic variants of the *Runx2* gene are associated with femoral neck BMD in Spanish women. J Bone Miner Metab 28:696–705 (2010).

Sears KE, Goswami A, Flynn JJ, Niswander LA: The correlated evolution of *Runx2* tandem repeats, transcriptional activity, and facial length in carnivora. Evol Dev 9:555–565 (2007).

Vaughan T, Pasco JA, Kotowicz MA, Nicholson GC, Morrison NA: Alleles of *RUNX2/CBFA1* gene are associated with differences in bone mineral density and risk of fracture. J Bone Miner Res 17:1527–1534 (2002).

Vaughan T, Reid DM, Morrison NA, Ralston SH: *RUNX2* alleles associated with BMD in Scottish women; interaction of *RUNX2* alleles with menopausal status and body mass index. Bone 34:1029–1036 (2004).

Yoshida CA, Furuichi T, Fujita T, Fukuyama R, Kanatani N, et al: Core-binding factor beta interacts with Runx2 and is required for skeletal development. Nat Genet 32:633–638 (2002).

Brief Report—Endocrine Research

C-type natriuretic peptide (CNP) plasma levels are elevated in subjects with achondroplasia, hypochondroplasia, and thanatophoric dysplasia

Robert C. Olney,[1] Timothy C.R. Prickett [2], Eric A. Espiner,[2] William G. Mackenzie,[3] Angela L. Duker,[3] Colleen Ditro,[3] Bernhard Zabel,[4] Tomonobu Hasegawa[5], Hiroshi Kitoh,[6] Arthur S. Aylsworth,[7] Michael B. Bober[3]

[1]Nemours Children's Clinic, Jacksonville, FL; [2] University of Otago, Christchurch, New Zealand; [3]Nemours/Alfred I. duPont Hospital for Children, Wilmington, DE [4]University Hospital Freiburg, Freiburg, Germany; [5]Keio University School of Medicine, Tokyo, Japan; [6]Nagoya University School of Medicine, Nagoya, Japan; [7]University of N Carolina, Chapel Hill, NC

Context: C-type natriuretic peptide (CNP) is a crucial regulator of endochondral bone growth. In a previous report of a child with acromesomelic dysplasia, Maroteaux type (AMDM), due to loss-of-function of the CNP receptor (NPR-B), plasma levels of CNP were elevated. In vitro studies have shown that activation of the MEK/ERK MAP kinase pathway causes functional inhibition of NPR-B. Achondroplasia, hypochondroplasia, and thanatophoric dysplasia are syndromes of short-limbed dwarfism caused by activating mutations of fibroblast growth factor receptor-3, which result in over-activation of the MEK/ERK MAP kinase pathway.

Objective: To determine if these syndromes exhibit evidence of CNP resistance as reflected by increases of plasma CNP and its amino terminal propeptide (NTproCNP).

Design: This was a prospective, observational study.

Subjects: Participants were 63 children and 20 adults with achondroplasia, 6 children with hypochondroplasia, 2 children with thanatophoric dysplasia, and 4 children and 1 adult with AMDM.

Results: Plasma levels of CNP and NTproCNP were higher in children with achondroplasia with CNP SD scores (SDS) of 1.0 (0.3–1.4) [median (intraquartile range)] and NTproCNP SDS of 1.4 (0.4–1.8) ($p<0.0005$). NTproCNP levels correlated with height velocity. Levels were also elevated in adults with achondroplasia, CNP SDS 1.5 (0.7–2.1) and NTproCNP SDS 0.5 (0.1–1.0), $p<0.005$. In children with hypochondroplasia, CNP SDS were 1.3 (0.7–1.5)($p=0.08$) and NTproCNP SDS were 1.9 (1.8–2.3)($p<0.05$). In children with AMDM, CNP SDS were 1.6 (1.4–3.3) and NTproCNP SDS were 4.2 (2.7–6.2) ($p<0.01$).

Conclusions: In these skeletal dysplasias, elevated plasma levels of proCNP products suggest the presence of tissue resistance to CNP.

C-type natriuretic peptide (CNP) is a member of the natriuretic peptide family that includes atrial natriuretic peptide and B-type natriuretic peptide. The cognate receptor for CNP is natriuretic peptide receptor-B (NPR-B, gene NPR2), a membrane receptor that generates cyclic GMP as the second messenger. C-type natriuretic peptide is produced in the growth plate and is a potent positive regulator of linear growth (reviewed in 1). Homozygous or biallelic inactivating mutations of NPR2 cause acromesomelic dysplasia, Maroteaux type (MIM 602 875, AMDM), a form of short-limbed dwarfism (2).

C-type natriuretic peptide levels can be measured in

ISSN Print 0021-972X ISSN Online 1945-7197
Printed in U.S.A.

Received July 1, 2014. Accepted November 6, 2014.

Abbreviations:

plasma, although specific clearance pathways result in low levels. Biosynthetic processing of CNP generates an amino-terminal propeptide (NTproCNP) that is released from the cell in an equimolar ratio to CNP. This propeptide is not subject to specific clearance pathways. As a result, plasma NTproCNP levels reflect CNP production more accurately than levels of the active peptide (3). In a previous report, we documented greatly elevated plasma concentrations of CNP and NTproCNP in a child with AMDM (1), suggesting that reduced intracellular CNP pathway activity may increase CNP production.

Achondroplasia (MIM 100 800) is the most common skeletal dysplasia with incidence estimates ranging from 1 in 15 000 to 1 in 26 000 births (4). Achondroplasia is caused by a mutation in the fibroblast growth factor receptor-3 gene (FGFR3) (5). A single mutation (G380R) accounts for greater than 98% of all reported cases of achondroplasia and is a gain-of-function mutation. Hypochondroplasia (MIM 146 000) is a related, but milder skeletal dysplasia. Thanatophoric dysplasia (MIM 187 600) is a rarer syndrome of skeletal dysplasia, with phenotypic features more severe than in achondroplasia and is often lethal in the neonatal period. Both hypochondroplasia and thanatophoric dysplasia are also caused by gain-of-function mutations in FGFR3 (6, 7).

In the growth plate, FGFR-3 activates a number of signaling cascades, the most important of which appear to be the signal transducers and activators of transcription (STAT1) pathway, which inhibits chondrocyte proliferation, and the MEK/ERK mitogen-activated protein kinase (MAP kinase) pathway, which inhibits chondrocytic differentiation and increases matrix degradation. The net result is poor bone growth (reviewed in 8). The MEK/ERK MAP kinase pathway and the CNP intracellular signaling pathway interact and are mutually inhibitory (9). Evidence of functional inhibition of NPR-B by FGFR-3 overactivity, and our finding of raised plasma CNP peptides in a patient with a homozygous loss-of-function mutation in NPR2, lead us to postulate that plasma levels will also be raised in disorders associated with constitutive activation of FGFR-3.

Materials and Methods

Subjects

Subjects were healthy people with the clinical diagnosis of achondroplasia (63 children, 20 adults), hypochondroplasia (6 children), thanatophoric dysplasia (2 children), or AMDM (4 children and 1 adult). This study was approved by the Nemours Florida Institutional Review Board. All children had written parental permission obtained. All adult subjects had written informed consent obtained.

Study procedures

With the exception of AMDM, this was a prospective study. All subjects with achondroplasia, hypochondroplasia, or thanatophoric dysplasia were seen in the Skeletal Dysplasia Clinic at Nemours/Alfred I. duPont Hospital for Children in Wilmington, DE. Anthropometrics were done, including standing height by wall-mounted tape measure or recumbent length by measuring table and weight by electronic scale. If the subject was an established patient, heights from previous visits were obtained from the medical record for determination of annualized height velocity.

Subjects with AMDM were seen by a variety of geneticists around the world. Blood was drawn locally and plasma was frozen and shipped for analysis.

Assays

Blood was drawn into EDTA tubes and stored at 4 C until processed. Blood was centrifuged at 4 C and plasma aliquoted and frozen at −80 C until assayed.

The radioimmunoassays used for CNP and NTproCNP were as previously described (10, 11).

Statistical analysis

Standard deviation scores (SDS) were calculated using the LMS method (12). Height SDS were calculated using Center for Disease Control 2000 data (13). For the subjects with AMDM residing outside the US, country specific height data were used. Standard deviation scores for CNP, NTproCNP, and CNP-to-NTproCNP ratio were calculated using reference data from our previous studies of healthy children (10) and adults (11). Achondroplasia-specific height SDS were calculated using estimates of age-specific mean and SD from height charts reported by Horton, et al (14).

Data are summarized as median and interquartile range (25th - 75th percentiles). For height SDS data, one sample Student's t-tests were used to compare groups to the general population. For the peptide assay data, because of the widely differing ranges of variance in the sample groups, nonparametric tests were used. For the children, comparison between the reference population, and subjects with achondroplasia, hypochondroplasia, or AMDM were made using Kruskal-Wallis tests, with Holm-adjusted Mann-Whitney rank sum tests for post hoc pairwise comparisons. For the adults, comparison of SDS data were made using Mann-Whitney rank sum tests. Correlation between NTproCNP level and height velocity were done by fitting a line by least squares and performing linear regression analysis. Pearson product-moment correlation coefficients (r) are reported. Statistics where calculated using Primer of Biostatistics software (version 7; The McGraw-Hill Companies, Inc., New York, NY). Significance was assumed for p values less than 0.05.

Results

Achondroplasia

The characteristics of the subjects with achondroplasia are shown in Table 1. In children with achondroplasia, plasma concentration of both CNP and NTproCNP (Figure 1) were higher than in the reference population ($P <$

Table 1. Subjects with Achondroplasia or Hypochondroplasia

	Achondroplasia		Hypochondroplasia
	children	**adults**	**children**
number	63	20	6
sex (F:M)	31:32	11:9	3:3
age (y)	4.7 (2.9–7.5)	41 (36–45)	8.6 (6.6–10.9)
height SD score[a]	−4.8 (-5.6- −4.2)**	ND	−3.1 (-3.7- −2.2)*†
height SD score[b]	−0.1 (-0.8–0.5)	ND	1.9 (1.3–3.0)†
CNP (pM)	2.1 (1.7–2.4)	0.9 (0.7–1.1)	2.3 (1.9–2.5)
CNP SD score	1.0 (0.3–1.4)**	1.5 (0.7–2.1)*	1.3 (0.7–1.5)*
NTproCNP (pM)	53.0 (47.3–63.0)	17.0 (16.0–19.3)	55.2 (52.1–58.7)
NTproCNP SD score	1.4 (0.4–1.8)**	0.5 (0.1–1.0)*	1.9 (1.8–2.3)*
NTproCNP:CNP ratio	26 (31–22)	21 (16–36)	23 (25–22)
NTproCNP:CNP SD score	−0.1 (-0.7–0.4)	−0.9 (-1.6–0.4)	0.2 (-0.4–0.2)

Data are median (intraquartile range)

ND, not determined

[a]Using general population reference standards

[b]Using achondroplasia-specific reference standards

*$P < 0.01$ compared to the reference population

**$P < 0.0005$ compared to the reference population

†$P < 0.01$, compared to subjects with achondroplasia

.0005 for both), despite markedly reduced height. Similarly, adults with achondroplasia also had higher levels of CNP and NTproCNP ($P < .005$ for both)(Table 1). The NTproCNP-to-CNP ratio is a measure of CNP clearance and did not differ from the reference population (Table 1).

Linear regression analysis showed that in children with achondroplasia, NTproCNP level had a significant positive correlation with height velocity (n = 62, $r^2=0.42$, $P < .0005$)(Figure 1, panel C). A similar relationship was found in the reference population (n = 139, $r^2=0.51$, $P < .0005$) (10). The regression line for children with achondroplasia differed from that of the reference population both for slope (1.76 ± 0.27 vs. 2.41 ± 0.20 pM/cm/y respectively, mean±SE, $P < .05$) and for intercept (46.7 ± 2.3 vs. 24.1 ± 1.3 pM, $P < .0005$).

Hypochondroplasia

Table 1 shows the characteristics of the subjects with hypochondroplasia, all of whom were children. Compared to the reference population, these subjects had elevated plasma CNP and NTproCNP levels (Figure 1)($P < .05$ for both). Compared to subjects with achondroplasia, the CNP and NTproCNP SDS were not different (Figure 1).

Thanatophoric dysplasia

We studied two young children with thanatophoric dysplasia. One subject was a 2.3 year old boy with a height SDS of −11.5. His plasma CNP level was 3.0 pM (SDS of 3.0) and his NTproCNP level was 67.3 (SDS of 1.1). The second subject was a 2.7 year old boy with a height SDS of −11.1. His plasma CNP level was 1.0 pM (SDS of 0.0) and his NTproCNP level was 72.2 (SDS of 1.8).

Acromesomelic dysplasia, Maroteaux type

Table 2 shows the characteristics of subjects with AMDM. In the children, CNP SDS (n = 3, $P < .01$) and NTproCNP SDS (n = 4, $P < .005$) were significantly higher than in the reference population and were also higher than values in achondroplasia (CNP SDS, $P < .05$; NTproCNP SDS, $P < .005$, Figure 1). In the adult with AMDM, both plasma CNP and NTproCNP were markedly elevated.

Discussion

The finding that CNP products in plasma were greatly elevated in a subject with profound short stature due to a disruption of the CNP receptor (NPR-B) and reports from others that activation of the MEK/ERK MAP kinase pathway inhibits NPR-B signaling, lead us to postulate that plasma levels would also be elevated in people with FGFR-3-related skeletal dysplasias such as achondroplasia. The current findings clearly show that circulating products of proCNP are raised not only in children and adults with achondroplasia, but also in children with related conditions of FGFR-3 overactivity.

People with AMDM have absent or disrupted CNP receptors. Since CNP is a growth promoting factor and people with AMDM have profound growth failure, this is a classic instance of hormone resistance. We have shown

Table 2. Subjects with Acromesomelic Dysplasia, Maroteaux Type

Age (y)	Genotype	Sex	height SDS	CNP (pM)	CNP SDS	NTproCNP (pM)	NTproCNP SDS	NT:CNP	NT:CNP SDS
2.5	G413E/G413E	M	−5.1	2.7	1.6	86.3	2.8	32.0	−0.5
4.9	del/del	M	−5.3	ND	ND	110.2	5.6		
7.5	R668stop/R218C	F	−2.3	2.1	1.1	58.0	2.4	27.6	−0.6
7.9	I364fs/I364fs	F	−8.5	7.6	5.0	172.0	7.9	22.6	0.1
30	Q853stop/R989 liter	M	−8.6	7.8	46.6	144.0	8.0	18.5	−1.7

ND, not determined

here that CNP and NTproCNP levels are markedly elevated in people with AMDM, suggesting that CNP, as in virtually all other hormone axes, is regulated by a negative feedback loop. Supporting this conclusion are two reports of subjects with activating mutations of NPR-B causing skeletal overgrowth (15, 16), in whom plasma NTproCNP concentrations were profoundly reduced. Little is known about the factors that regulate CNP expression and translation; the details of this feedback loop require further study.

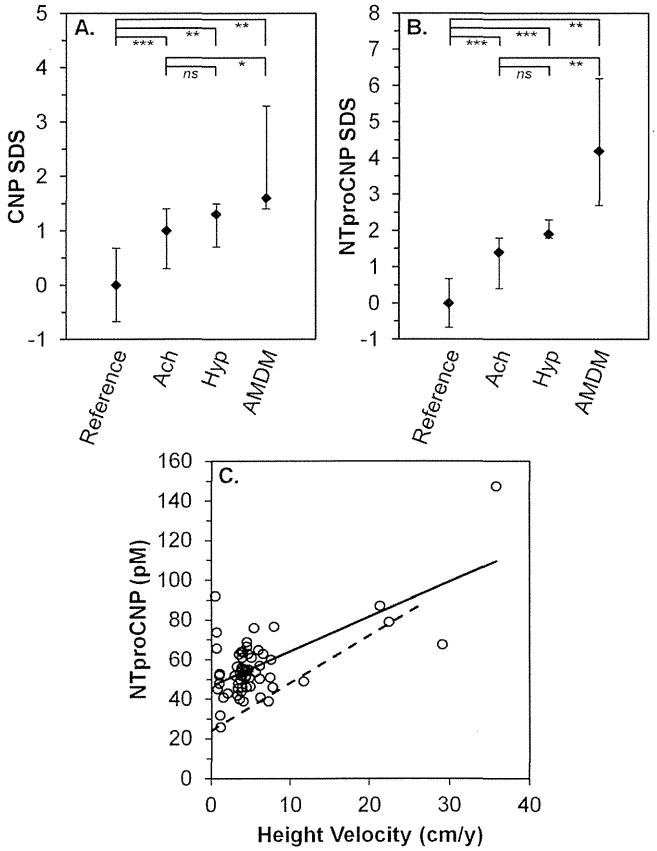

Figure 1. C-type natriuretic peptide and NTproCNP levels in children. Panels A & B, comparison between different skeletal dysplasias. Standard deviation scores are shown for CNP (Panel A) and NTproCNP (Panel B) for children from the reference population (n = 318), children with achondroplasia (n = 63, Ach), hypochondroplasia (n = 6, Hyp), and acromesomelic dysplasia, Maroteaux-type (n = 4, AMDM). Diamonds show the median for each group and error bars the 25th and 75th percentile. ns, difference is not significant. $*P < .05$; $**P < .01$; $***P < .0005$. Panel C shows the correlation between height velocity and NTproCNP levels in children with achondroplasia. Annualized height velocity was determined using the height at a previous clinic visit and the height from the study visit. Solid line, least mean squares linear regression line. The correlation is significant (n = 62, $r^2=0.416$, $P < .0005$). Dashed line, previously published regression line from children from the general population (n = 139, r = 0.711, $P < .0005$) (10). The two regression lines differ both in intercept ($P < .05$) and in slope ($P < .0005$).

The interaction between the MEK/ERK MAP kinase and CNP/cGMP pathways has been defined in vitro in chondrogenic cell systems and in organ culture. Phosphorylated MEK1/2 and/or ERK1/2 directly or indirectly inhibit cGMP generation by NPR-B (9). Meanwhile, NPR-B-generated cGMP, in a pathway that involves cGMP-dependent protein kinase II (PRKG2) and the MKK/p38 MAP kinase pathway, inhibits MEK/ERK activation by inhibiting RAF1 (17, 9, 18, 19). Hence in vitro data describe a potential mechanism in which overactivation of the MEK/ERK MAP kinase pathway can result in resistance to CNP.

In this study, we observed a clear increase in CNP and NTproCNP levels in subjects with achondroplasia and hypochondroplasia. We also provide evidence for increased levels in two children with thanatophoric dysplasia, although the sample size was too small for statistical confirmation. Assuming the presence of CNP regulatory feedback loop as suggested by the data from subjects with AMDM, the finding of elevated CNP levels in a population with severe short stature suggests that these individuals may also have resistance to CNP. This is further demonstrated by Figure 1 (panel C), which shows that the slope of the regression line linking NTproCNP and height velocity is significantly reduced in children with achondroplasia compared to the reference population.

There are other potential explanations for our findings. It may be that another branch of the FGFR-3 signaling cascade up-regulates CNP expression and that the MAP kinase inhibition of NPR-B signaling is not occurring or is not relevant in vivo. Another possibility is that the elevated blood levels of CNP are arising from other tissues and not the growth plate and hence not relevant to the growth failure. Now that the observation has been made, further definition is needed to provide clarity. Of interest, products of proCNP in plasma are also elevated in adults with

achondroplasia or AMDM. The tissues that contribute to plasma levels of CNP and NTproCNP after growth plates have closed have not been clearly defined, but are likely to include skeletal, vascular, and cardiac (11, 20) tissue. C-type natriuretic peptide, NPR-B, and FGFR-3 are all expressed in these tissues. The finding of elevated plasma levels of CNP in adults with achondroplasia suggests that alteration of the CNP pathway by activating FGFR3 mutations is not limited to the growth plate.

Acknowledgments

The authors would like to thank the subjects and their families for participating in this project.

Address all correspondence and requests for reprints to: Robert C. Olney, MD, Nemours Children's Clinic, Jacksonville, FL 32 207, (904) 697–3674 fax: (904) 697–3948, rolney@nemours.org.

Disclosure summary: T.C.R.P. and E.A.E. have a patent filed entitled "Assessment of skeletal growth using measurements of NT-CNP peptides"

Clinical Trial Registration Number: NCT01541306

Reprint requests: to corresponding author

This work was supported by Support: developmental funds from Nemours.

References

1. **Olney RC.** C-type natriuretic peptide in growth: a new paradigm. *Growth Horm IGF Res.* 2006;16 Suppl A:S6–14.
2. **Bartels CF, Bukulmez H, Padayatti P, Rhee DK, Ravenswaaij-Arts C, Pauli RM, Mundlos S, Chitayat D, Shih LY, Al Gazali LI, Kant S, Cole T, Morton J, Cormier-Daire V, Faivre L, Lees M, Kirk J, Mortier GR, Leroy J, Zabel B, Kim CA, Crow Y, Braverman NE, van den Akker F, Warman ML.** Mutations in the Transmembrane Natriuretic Peptide Receptor NPR-B Impair Skeletal Growth and Cause Acromesomelic Dysplasia, *Type Maroteaux. Am J Hum Genet.* 2004;75:27–34.
3. **Prickett TCR, Espiner EA.** 2012 C-type natriuretic peptide (CNP) and postnatal linear growth. 2789–2810.
4. **Hunter AG, Bankier A, Rogers JG, Sillence D, Scott CI, Jr.** Medical complications of achondroplasia: a multicentre patient review. *J Med Genet.* 1998;35:705–712.
5. **Shiang R, Thompson LM, Zhu YZ, Church DM, Fielder TJ, Bocian M, Winokur ST, Wasmuth JJ.** Mutations in the transmembrane domain of FGFR3 cause the most common genetic form of dwarfism, achondroplasia. *Cell.* 1994;78:335–342.
6. **Bellus GA, McIntosh I, Smith EA, Aylsworth AS, Kaitila I, Horton WA, Greenhaw GA, Hecht JT, Francomano CA.** A recurrent mutation in the tyrosine kinase domain of fibroblast growth factor receptor 3 causes hypochondroplasia. *Nat Genet.* 1995;10:357–359.
7. **Tavormina PL, Shiang R, Thompson LM, Zhu YZ, Wilkin DJ, Lachman RS, Wilcox WR, Rimoin DL, Cohn DH, Wasmuth JJ.** Thanatophoric dysplasia (types I and II) caused by distinct mutations in fibroblast growth factor receptor 3. *Nat Genet.* 1995;9:321–328.
8. **Foldynova-Trantirkova S, Wilcox WR, Krejci P.** Sixteen years and counting: the current understanding of fibroblast growth factor receptor 3 (FGFR3) signaling in skeletal dysplasias. *Hum Mutat.* 2012;33:29–41.
9. **Ozasa A, Komatsu Y, Yasoda A, Miura M, Sakuma Y, Nakatsuru Y, Arai H, Itoh N, Nakao K.** Complementary antagonistic actions between C-type natriuretic peptide and the MAPK pathway through FGFR-3 in ATDC5 cells. *Bone.* 2005;36:1056–1064.
10. **Olney RC, Permuy JW, Prickett TC, Han JC, Espiner EA.** Amino-terminal propeptide of C-type natriuretic peptide (NTproCNP) predicts height velocity in healthy children. *Clin Endocrinol (Oxf).* 2012;77:416–422.
11. **Prickett TC, Olney RC, Cameron VA, Ellis MJ, Richards AM, Espiner EA.** Impact of age, phenotype and cardio-renal function on plasma C-type and B-type natriuretic peptide forms in an adult population. *Clin Endocrinol (Oxf).* 2013;78:783–789.
12. **Cole TJ.** The LMS method for constructing normalized growth standards. *Eur J Clin Nutr.* 1990;44:45–60.
13. **National Center for Health Statistics 2002 2000 CDC Growth Charts for the United States: Methods and Development. Vital and Health Statistics 11:1–203.**
14. **Horton WA, Rotter JI, Rimoin DL, Scott CI, Hall JG.** Standard growth curves for achondroplasia. *J Pediatr.* 1978;93:435–438.
15. **Miura K, Namba N, Fujiwara M, Ohata Y, Ishida H, Kitaoka T, Kubota T, Hirai H, Higuchi C, Tsumaki N, Yoshikawa H, Sakai N, Michigami T, Ozono K.** An Overgrowth Disorder Associated with Excessive Production of cGMP Due to a Gain-of-Function Mutation of the Natriuretic Peptide Receptor 2 Gene. *PLoS One.* 2012;7:e42180.
16. **Hannema SE, van Duyvenvoorde HA, Premsler T, Yang RB, Mueller TD, Gassner B, Oberwinkler H, Roelfsema F, Santen GW, Prickett T, Kant SG, Verkerk AJ, Uitterlinden AG, Espiner E, Ruivenkamp CA, Oostdijk W, Pereira AM, Losekoot M, Kuhn M, Wit JM.** An activating mutation in the kinase homology domain of the natriuretic peptide receptor-2 causes extremely tall stature without skeletal deformities. *J Clin Endocrinol Metab.* 2013;98:E1988–E1998.
17. **Yasoda A, Komatsu Y, Chusho H, Miyazawa T, Ozasa A, Miura M, Kurihara T, Rogi T, Tanaka S, Suda M, Tamura N, Ogawa Y, Nakao K.** Overexpression of CNP in chondrocytes rescues achondroplasia through a MAPK-dependent pathway. *Nat Med.* 2004;10:80–86.
18. **Krejci P, Masri B, Fontaine V, Mekikian PB, Weis M, Prats H, Wilcox WR.** Interaction of fibroblast growth factor and C-natriuretic peptide signaling in regulation of chondrocyte proliferation and extracellular matrix homeostasis. *J Cell Sci.* 2005;118:5089–5100.
19. **Hutchison MR.** BDNF alters ERK/p38 MAPK activity ratios to promote differentiation in growth plate chondrocytes. *Mol Endocrinol.* 2012;26:1406–1416.
20. **Palmer SC, Prickett TC, Espiner EA, Yandle TG, Richards AM.** Regional release and clearance of C-type natriuretic peptides in the human circulation and relation to cardiac function. *Hypertension.* 2009;54:612–618.

Original Article

DOI: 10.5582/irdr.2014.01009

Radiographic characteristics of the hand and cervical spine in fibrodysplasia ossificans progressiva

Kenichi Mishima[1], Hiroshi Kitoh[1,2,*], Nobuhiko Haga[2], Yasuharu Nakashima[2], Junji Kamizono[2], Takenobu Katagiri[2], Takafumi Susami[2], Masaki Matsushita[1], Naoki Ishiguro[1]

[1] *Department of Orthopaedic Surgery, Nagoya University Graduate School of Medicine, Nagoya, Aichi, Japan;*
[2] *The Research Committee on Fibrodysplasia Ossificans Progressiva, Tokyo, Japan.*

Summary **Fibrodysplasia ossificans progressiva (FOP) is a disabling heritable disorder of connective tissue characterized by progressive heterotopic ossification in various extraskeletal sites. Early correct diagnosis of FOP is important to prevent additional iatrogenic harm or trauma. Congenital malformation of the great toes is a well-known diagnostic clue, but some patients show normal-appearing great toes. The thumb shortening and cervical spine abnormalities are other skeletal features often observed in FOP. This study aimed to address the quantitative assessment of these features in a cohort of patients with FOP, which potentially helps early diagnosis of FOP. Radiographs of the hand and cervical spine were retrospectively analyzed from a total of 18 FOP patients (9 males and 9 females) with an average age of 13.9 years (range 0.7-39.3 years). The elevated ratio of the second metacarpal bone to the distal phalanx of the thumb (> +1SD) was a consistent finding irrespective of the patient's age and gender. Infant FOP patients, in addition, exhibited an extremely high ratio of the second metacarpal bone to the first metacarpal bone (> +3SD). The height/depth ratio of the C5 vertebra increased in patients over 4 years of age (> +2SD). Additionally, the ratio of (height+depth) of the C5 spinous process to the C5 vertebral depth was markedly elevated in young patients (> +2SD). We quantitatively demonstrated the hand and cervical spine characteristics of FOP. These findings, which can be seen from early infancy, could be useful for early diagnosis of FOP even in patients without great toe abnormalities.**

Keywords: Fibrodysplasia ossificans progressiva, early diagnosis, radiographic characteristics

1. Introduction

Fibrodysplasia ossificans progressiva (FOP) is a severely disabling genetic disorder of connective tissues characterized by congenital malformations of the great toes and progressive heterotopic ossification (HO) in various extraskeletal sites including muscles, tendons, ligaments, fascias, and aponeuroses. FOP is caused by a recurrent activating mutation (c.617G > A, p.R206H) in the gene encoding activin receptor IA/activin-like kinase 2 (ACVR1/ALK2), a bone morphogenetic protein (BMP) type I receptor (*1*). HO typically begins to form during the first decade of life preceded by painful soft tissue swelling and inflammation (flare-ups), which are sometimes mistaken for aggressive fibromatosis or musculoskeletal tumors. Surgical resection of HO leads to explosive new bone formation (*2*). Since there is no definitive treatment to prevent progressive HO in FOP to date (*3*), early correct diagnosis is necessary to maintain their mobility by preventing additional iatrogenic harm (*4*).

Malformations of the great toes, such as hallux valgus, deformed proximal phalanges and shortened first metatarsal bones, are well-known pre-osseous features of FOP (*5*). A reported incidence of these deformities is 95%, suggesting that there exists rare FOP cases without the great toe abnormalities (*6*). We demonstrated additional early radiographic signs of FOP including shortening of the first metacarpal bones and hypertrophy of the posterior element of the cervical

**Address correspondence to:*
Dr. Hiroshi Kitoh, Department of Orthopaedic Surgery, Nagoya University Graduate School of Medicine, 65 Tsurumai, Showa-ku, Nagoya, Aichi, 466-8550, Japan.
E-mail: hkitoh@med.nagoya-u.ac.jp

spine (*7*). Clinical awareness of these deformities can aid clinicians in making early diagnosis of FOP, but quantitative assessment of these deformities has not yet been determined.

In this study, we retrospectively examined radiographs of the hand and cervical spine in FOP patients and demonstrated various abnormal radiographic parameters helpful for early diagnosis of this specific disorder.

2. Materials and Methods

2.1. *Demographics*

This study represents a retrospective case-control study consisting of Japanese FOP patients followed up at health care facilities where members of the Research Committee on Japanese Fibrodysplasia Ossificans Progressiva practiced. After approval from the Institutional Review Board of the Nagoya University Hospital, we collected the hand and/or cervical spine radiographs from 18 FOP patients (9 males and 9 females) with an average age of 13.9 years (range 0.7-39.3 years) at the time of this study. The patients were diagnosed clinically and radiographically based on various characteristic findings of FOP including deformities of the great toes, extraskeletal HO, joint contractures, cervical fusions, broad femoral necks, and osteochondroma-like lesions. Molecular testing was performed on fourteen patients. Thirteen showed the common *ACVR1/ALK2* mutation within the glycine/serine-rich regulatory (GS) domain (c.617G > A, p.R206H), and one patient had an atypical mutation within the protein kinase domain (c.774G > T, p.R258S). Molecular studies were not conducted for the remaining 4 patients who showed characteristic skeletal features of FOP. We examined anteroposterior (AP) radiographs of the hands and lateral radiographs of the cervical spine in each individual. The earliest hands and cervical spine films were analyzed using image processing and analysis software ImageJ®.

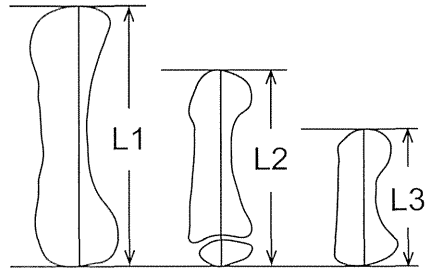

Figure 1. A schematic diagram illustrating the measurement method of bone length in the hand. Bone length was defined as the distance between the tangents drawn to each end of the bone, which were perpendicular to the bone axis. The entire bone length was measured for adults (L1), children (L2), and infants (L3).

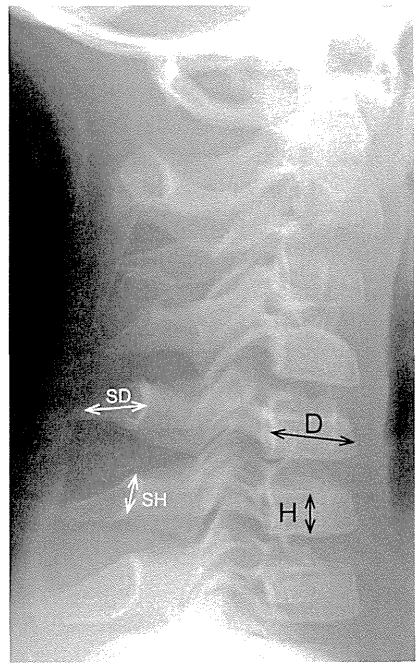

Figure 2. A radiograph depicting the measurements of the bone length in the cervical spine. The height (H) and depth (D) of the C5 vertebral body was measured at the midportion of the body. The height of the C5 spinous process (SH) was defined as the distance from the cranial to the caudal rim at the juxta-laminar zone. The depth of the spinous process (SD) was measured from the midpoint of the anterior wall to that of the posterior rim.

2.2. *Radiographic assessment of the hand*

According to the measurement method by Poznanski *et al.* (*8*), the length of each phalanx and metacarpal bone was measured. In brief, the tangent lines were drawn at both ends of each bone, which were perpendicular to the bone axis, and a bone length was defined as the distance between these two lines (Figure 1). We measured a length of the distal (D1) and proximal (P1) phalanges of the thumb as well as that of the first and second metacarpal bones (MET1 and MET2), and calculated the following bone length ratios, MET2/MET1, MET2/P1, MET2/D1, MET1/P1, MET1/D1, and P1/D1. Radiographs of both hands from one patient were separately analyzed to obtain the average value of the measurements. Reference ranges of these measurements in different ages and genders were used based on the literature from Poznanski *et al.* (*8*). The control data of these measurements in infant (n = 21) were determined by the radiographic database in Nagoya University Hospital.

2.3. *Radiographic assessment of the cervical spine*

According to the measurement method proposed by Remes *et al.* (*9*), the height and depth of the C5 vertebral body were measured. Briefly, vertebral body height (H) was measured at the midpoint of the vertebra, perpendicular to the lower end plate. The vertebral body depth (D) was measured at the midpoint of the body from the anterior wall to the posterior wall (Figure 2). The H/D ratios of the C5 vertebra were then calculated

Table 1. Characteristics and quantitative indices for the study population

Patient	Sex	ALK2 mutation	Age at X-ray (yrs)	Deviation of the bone length ratios (SD)			
			Hand/Cervical spine	MET2/D1	MET2/D1	H/D	(SH+SD)/D
1	M	R206H	0/0	1.0	1.0	0.6	0.1
2	M	R206H	0/0	2.4	2.4	0.6	7.1
3	M	R206H	1/3	3.1	3.1	0.9	2.8
4	F	R206H	5/6	2.8	2.8	3.3	8.3
5	M	R206H	8/7	6.2	6.2	2.8	3.7
6	M	R206H	12/18	4.1	4.1	1.9	1.5
7	F	R206H	17/17	4.0	4.0	4.1	NA
8	F	R206H	20/NA	2.2	2.2	NA	NA
9	M	R206H	29/NA	2.7	2.7	NA	NA
10	M	R206H	34/NA	3.5	3.5	NA	NA
11	F	R206H	36/NA	1.0	1.0	NA	NA
12	M	R206H	39/16	1.9	1.9	3.0	1.8
13	F	R206H	NA/18	NA	NA	0.6	2.4
14	F	R258S	14/14	1.7	1.7	4.9	NA
15	M	ND	NA/4	NA	NA	3.2	8.8
16	F	ND	NA/8	NA	NA	9.2	7.9
17	F	ND	NA/16	NA	NA	4.4	NA
18	F	ND	5/5	5.3	5.3	5.3	5.4

M denotes male; F, female; ND, not determined; NA, not applicable; SD, standard deviation.

and compared to normal reference values established by Remes *et al.* in different age and gender groups (*9*). In addition, we measured the height and depth of the C5 spinous process. The height of the spinous process (SH) was defined as the distance from the cranial to caudal margin at the junction of the spinous process and lamina. The depth of spinous process (SD) was measured from the midportion of the anterior wall to that of the posterior rim demarcating a thick cortex shadow (Figure 2). The sum of SH and SD measurements was used for the evaluation of spinous process size, then the (SH + SD)/D ratio of the C5 vertebra was calculated. Reference values of the (SH + SD)/D ratio were established from the radiographic database of normal controls in Nagoya University Hospital.

3. Results

3.1. *Characteristics of the study cohort*

Patients' characteristics and quantitative indices of the measurements are shown in Table 1. Deviation of the bone length ratios in the hand and cervical spine was calculated based on age-matched reference values.

3.2. *Radiographic characteristics of the hand*

Mean and standard deviation of the MET2/D1 and MET2/MET1 ratio in control infants (n = 21) are 2.9 ± 0.29 and 1.64 ± 0.08, respectively. Twenty-six hand radiographs from 14 patients (8 males and 6 females) were available. Regardless of age and gender, all FOP patients showed a MET2/D1 ratio larger than +1SD of normal controls (Figure 3A and 3B). In infant patients without an epiphyseal ossification center of the first metacarpal bone, the MET2/MET1 ratio was extremely

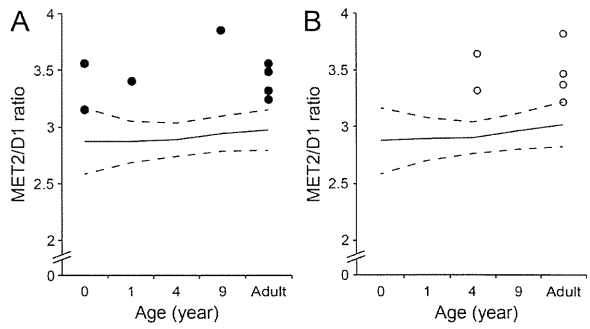

Figure 3. Scatter plots showing the bone length ratio of the second metacarpal bone (MET2) to the distal phalanx of the thumb (D1) in male (A) and female (B) patients with FOP. Solid and dash lines denote the normal value and the standard deviation (SD) of the MET2/D1 ratio, respectively.

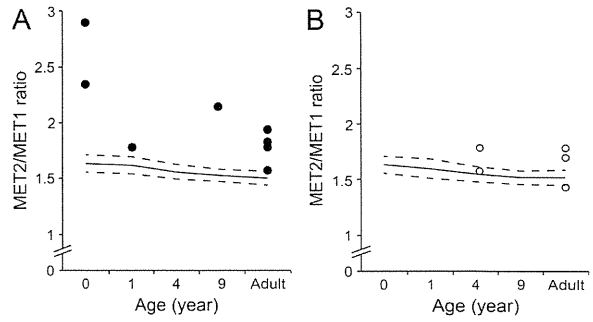

Figure 4. Scatter plots showing the bone length ratio of the second metacarpal bone (MET2) to the first metacarpal bone (MET1) in male (A) and female (B) patients with FOP. Solid and dash lines denote the normal value and the standard deviation (SD) of the MET2/MET1 ratio, respectively.

large (> +3SD of normal controls) (Figure 4A and 4B). The MET2/P1 ratio was higher in infant patients, but it scattered around the mean value with increasing age (data not shown). There were no characteristic features in the values of the MET1/P1, MET1/D1, and P1/D1 ratios in FOP patients, although the MET1/P1 and MET1/D1

Table 2. Mean and standard deviation of normal controls for the (SH+SD)/D ratio of the C5 vertebra

Age group	<1	1-2	2-3	3-4	4-5	5-6	6-7	7-8	8-9	9-10	10-11	11-12	12-13	13-14	14-15	15-16	16-17	17-18	18-19	19-20	20-21
Mean	1.05	1.10	1.09	1.20	1.21	1.43	1.37	1.47	1.33	1.47	1.50	1.53	1.51	1.57	1.69	1.86	1.76	1.73	1.71	1.78	1.86
SD	0.13	0.15	0.15	0.13	0.11	0.18	0.18	0.17	0.19	0.18	0.16	0.18	0.20	0.19	0.12	0.16	0.22	0.22	0.23	0.24	0.25
N	11	21	17	13	6	13	25	19	20	17	16	17	14	20	16	21	23	31	28	38	20

SD denotes standard deviation; N, number of control subjects; SH, height of the spinous process; SD, depth of the spinous process; D, depth of the vertebral body.

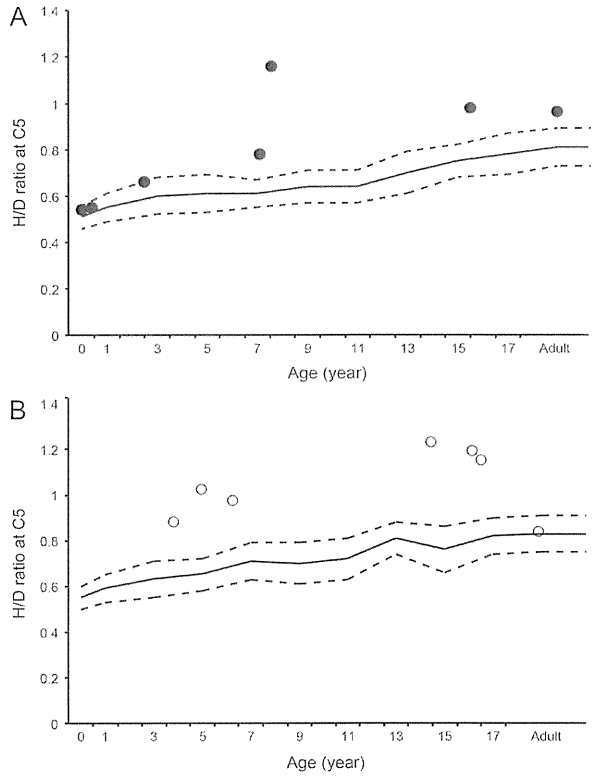

Figure 5. Scatter plots showing the bone length ratio of the C5 vertebral height (H) to depth (D) in male (A) and female (B) patients with FOP. Solid and dashed lines denote the normal value and the standard deviation (SD) of the H/D ratio, respectively.

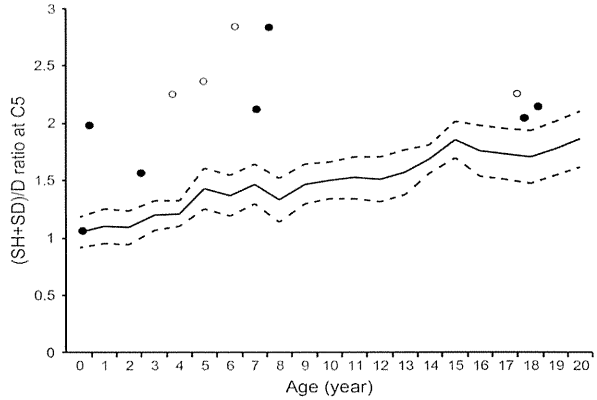

Figure 6. Scatter plots showing the bone length ratio of the C5 spinous process height (SH) + depth (SD) to the C5 vertebral depth (D). Solid and open circles indicate male and female, respectively. Solid and dashed lines denote the normal value and the standard deviation (SD) of the (SH+SD)/D ratio, respectively.

ratios were relatively small (< -1SD of normal controls) in infant FOP patients (data not shown).

3.3. *Radiographic characteristics of the cervical spine*

Reference values of the (SH + SD)/D ratio of the C5 vertebra are shown in Table 2. There were 14 (7 males and 7 females) cervical spine radiographs available for analysis. Among them, three radiographs were excluded from analysis of the (SH + SD)/D ratio for insufficient resolution. The H/D ratio of the C5 vertebra exceeded +2SD of normal controls in patients over 4 years of age except one female adult patient (Figure 5A and 5B). Similarly, the (SH + SD)/D ratio of the C5 vertebra was larger than +2SD of normal controls in young patients except one male infant (Figure 6).

4. Discussion

In the present study, we quantitatively proved the hand and cervical spine abnormalities in FOP including shortened thumbs as well as tall and narrow vertebral bodies and hypertrophic posterior elements of the cervical spine (*7,10*). Especially in young patients, shortening of the first metacarpal bone and enlargement of the cervical spinous processes were pathognomonic findings useful for early diagnosis of FOP before the appearance of HO.

Previous studies have reported that thumb shortening was seen in 50% of FOP patients (*6*). In the present study, all patients had a MET2/D1 ratio larger than +1SD of normal controls, and 85% (11/13) of the patients showed an increased MET2/MET1 ratio. The thumb shortening, therefore, seems to be more common than previous reports in FOP. Furthermore, an extremely high MET2/MET1 ratio in infant patients suggested that disproportionate shortening of the first metacarpal bone was an important early radiographic finding in FOP (Figure 7).

It is an intriguing feature of FOP that thumb morphogenesis is exclusively disrupted in the development of digit formation (*11*). The thumb is the last digit in the autopod to form, and it is different from other digits in terms of its relative position, shape, size, and number of phalanges. These unique thumb identities may be attributed to the expression profile of *HoxD* genes, which are pivotal transcriptional factors regulating limb patterning and growth (*12*). All four *HoxD10* to *D13* genes are expressed in the future digit II-V area in the autopod during the hand plate formation, whereas sole expression of the

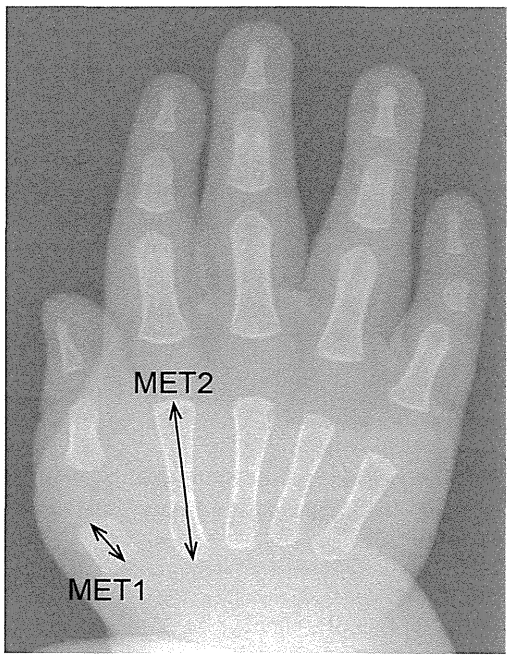

Figure 7. An anteroposterior radiograph of the right hand of Patient 1 at the age of eight months showing marked shortening of the first metacarpal bone. The MET2/MET1 ratio and the corresponding SD value is 2.9 and 16.3, respectively.

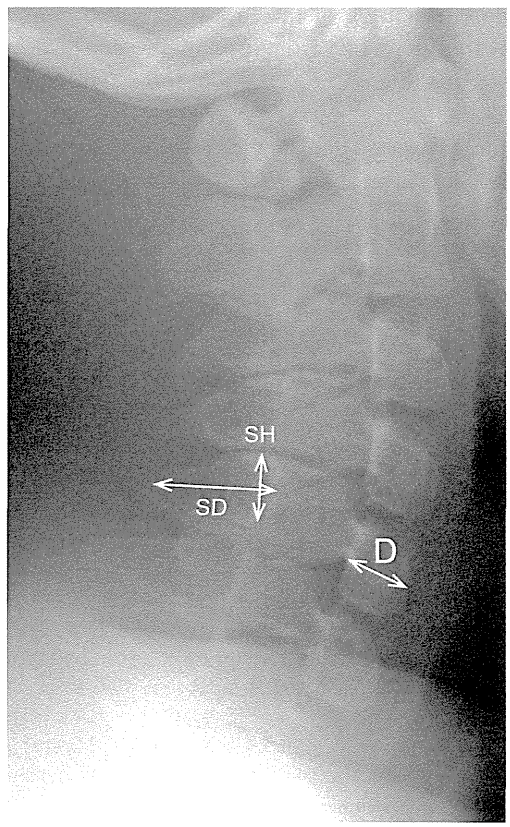

Figure 8. A lateral radiograph of the cervical spine of Patient 16 at the age of eight years showing enlarged spinous process of the C5 vertebra. The (SH+SD)/D ratio and the corresponding SD value is 2.8 and 7.9, respectively.

HoxD13 gene in the presumptive digit I area is of great significance (*13*). Mutations in the homeodomain of the *HoxD13* gene cause brachydactyly type D that is characterized by variable shortening of the distal phalanx of the thumb. This mutated HoxD13 proteins responsible for its decreased affinity for the double-stranded DNA target containing a cognitive sequence of the homeodomain (*14*). Interestingly, previous research has revealed that BMP signaling-dependent Smad1/4 proteins prevented HoxD10 and HoxD13 from binding to DNA targets (*15*). Constitutively-activated BMP signaling in FOP thus is likely to impair HoxD13-mediated transcriptional regulation by direct interactions between BMP-induced Smads and HoxD13. Mesenchymal condensation and chondrocyte proliferation of the presumptive digit I area could be suppressed by down-regulated HoxD13 function, whereas in presumptive digits II to V areas, it could be preserved by compensating expressions of other *HoxD* genes (*HoxD11* and *HoxD12*). Dysregulated BMP signal transduction during embryogenesis seems to cause relative shortening of the first metacarpals and distal phalanges of the thumb in FOP.

More than 90% of adult FOP patients showed fusion of the facet joints, which is a type of orthotopic ossification (*6*). To our knowledge, however, there are no reports delineating the precise prevalence of tall and narrow vertebral bodies and enlarged posterior elements of the cervical vertebrae. Here we demonstrated that the H/D and (SH + SD)/D ratios in the C5 vertebrae were larger than +2SD of normal values in 64% and 73% of patients, respectively (Figure 8). In addition to neck stiffness, which seemed to be an important early clinical sign before the appearance of HO (*6*), tall and narrow vertebrae and hypertrophic spinous processes of the cervical spine are radiographic characteristics in young FOP patients.

In a previous *in vivo* study, genetically-engineered overexpression of BMP-2/4 both dorsally and laterally to the neural tube manifested combined phenotypes of hypertrophic spinous processes and large deletion of the lateral and ventral parts of vertebral bodies (*16*). Thus, mesenchymal condensations at the paraxial mesoderm in FOP, where BMP-2 signaling is aberrantly activating, could be responsible for both enlarged spinous processes and relatively tall vertebral bodies.

The common *ACVR1/ALK2* mutation (c.617G > A, p.R206H) shows a homogeneous phenotype including congenital malformation of the great toes and the skeletal features in the thumb and cervical spine (*17*). In contrast, several atypical mutations in the *ALK2/ACVR1* gene, such as L196P, R258S, R375P, G328R, and P197_F198 del insL, have been identified in patients who showed normal-appearing great toes (*18*). In this study, one patient (Patient 14) with an atypical mutation (c.774G > C, p.R258S) showed normal-appearing great toes. She also lacked the shortened thumb but exhibited exceptionally tall and narrow vertebral bodies. Another patient (Patient 4) who showed neither malformed great

toes nor shortening of the first metacarpal bone also manifested distinctive features of the cervical spine in spite of the common *ACVR1/ALK2* mutation. We believe that radiographic characteristics of the cervical spine are potent diagnostic clues for FOP especially in cases without typical deformities of the great toes.

Acknowledgements

This work was supported partly by Research Committee on Fibrodysplasia Ossificans Progressiva from the Ministry of Health, Labour and Welfare of Japan.

References

1. Shore EM, Xu M, Feldman GJ, *et al.* A recurrent mutation in the BMP type I receptor ACVR1 causes inherited and sporadic fibrodysplasia ossificans progressiva. Nat Genet. 2006; 38:525-527.
2. Kitterman JA, Kantanie S, Rocke DM, Kaplan FS. Iatrogenic harm caused by diagnostic errors in fibrodysplasia ossificans progressiva. Pediatrics. 2005; 116:e654-e661.
3. Kitoh H, Achiwa M, Kaneko H, Mishima K, Matsushita M, Kadono I, Horowitz JD, Sallustio BC, Ohno K, Ishiguro N. Perhexiline maleate in the treatment of fibrodysplasia ossificans progressiva: An open-labeled clinical trial. Orphanet J Rare Dis. 2013; 8:163.
4. Pignolo RJ, Shore EM, Kaplan FS. Fibrodysplasia ossificans progressiva: Diagnosis, management, and therapeutic horizons. Pediatr Endocrinol Rev. 2013; 10 (Suppl 2):437-448.
5. Nakashima Y, Haga N, Kitoh H, Kamizono J, Tozawa K, Katagiri T, Susami T, Fukushi J, Iwamoto Y. Deformity of the great toe in fibrodysplasia ossificans progressiva. J Orthop Sci. 2010; 15:804-809.
6. Kaplan FS, Glaser DL, Shore EM, Deirmengian GK, Gupta R, Delai P, Morhart P, Smith R, Le Merrer M, Rogers JG, Connor JM, Kitterman JA. The phenotype of fibrodysplasia ossificans progressiva. Clin Rev Bone Miner Metab. 2005; 3:183-188.
7. Mishima K, Kitoh H, Katagiri T, Kaneko H, Ishiguro N. Early clinical and radiographic characteristics in fibrodysplasia ossificans progressiva: A report of two cases. J Bone Joint Surg Am. 2011; 93:e52.
8. Poznanski AK, Garn SM, Holt JF. The thumb in the congenital malformation syndromes. Radiology. 1971; 100:115-129.
9. Remes VM, Heinanen MT, Kinnunen JS, Marttinen EJ. Reference values for radiological evaluation of cervical vertebral body shape and spinal canal. Pediatr Radiol. 2000; 30:190-195.
10. Kaplan FS, Le Merrer M, Glaser DL, Pignolo RJ, Goldsby RE, Kitterman JA, Groppe J, Shore EM. Fibrodysplasia ossificans progressiva. Best Pract Res Clin Rheumatol. 2008; 22:191-205.
11. Pignolo RJ, Shore EM, Kaplan FS. Fibrodysplasia ossificans progressiva: Clinical and genetic aspects. Orphanet J Rare Dis. 2011; 6:80.
12. Oberg KC. Review of the molecular development of the thumb: Digit primera. Clin Orthop Relat Res. 2014; 472:1101-1105.
13. Deschamps J. Tailored *Hox* gene transcription and the making of the thumb. Genes Dev. 2008; 22:293-296.
14. Johnson D, Kan SH, Oldridge M, Trembath RC, Roche P, Esnouf RM, Giele H, Wilkie AO. Missense mutations in the homeodomain of HOXD13 are associated with brachydactyly types D and E. Am J Hum Genet. 2003; 72:984-997.
15. Li X, Nie S, Chang C, Qiu T, Cao X. Smads oppose Hox transcriptional activities. Exp Cell Res. 2006; 312:854-864.
16. Monsoro-Burq AH, Duprez D, Watanabe Y, Bontoux M, Vincent C, Brickell P, Le Douarin N. The role of bone morphogenetic proteins in vertebral development. Development. 1996; 122:3607-3616.
17. Kaplan FS, Xu M, Glaser DL, Collins F, Connor M, Kitterman J, Sillence D, Zackai E, Ravitsky V, Zasloff M, Ganguly A, Shore EM. Early diagnosis of fibrodysplasia ossificans progressiva. Pediatrics. 2008; 121:e1295-e1300.
18. Kaplan FS, Xu M, Seemann P, *et al.* Classic and atypical fibrodysplasia ossificans progressiva (FOP) phenotypes are caused by mutations in the bone morphogenetic protein (BMP) type I receptor ACVR1. Hum Mutat. 2009; 30:379-390.

(Received April 13, 2014; Revised April 24, 2014; Accepted May 07, 2014)

Original Article

DOI: 10.5582/irdr.2014.01009

Radiographic characteristics of the hand and cervical spine in fibrodysplasia ossificans progressiva

Kenichi Mishima[1], Hiroshi Kitoh[1,2,*], Nobuhiko Haga[2], Yasuharu Nakashima[2], Junji Kamizono[2], Takenobu Katagiri[2], Takafumi Susami[2], Masaki Matsushita[1], Naoki Ishiguro[1]

[1] *Department of Orthopaedic Surgery, Nagoya University Graduate School of Medicine, Nagoya, Aichi, Japan;*
[2] *The Research Committee on Fibrodysplasia Ossificans Progressiva, Tokyo, Japan.*

Summary **Fibrodysplasia ossificans progressiva (FOP) is a disabling heritable disorder of connective tissue characterized by progressive heterotopic ossification in various extraskeletal sites. Early correct diagnosis of FOP is important to prevent additional iatrogenic harm or trauma. Congenital malformation of the great toes is a well-known diagnostic clue, but some patients show normal-appearing great toes. The thumb shortening and cervical spine abnormalities are other skeletal features often observed in FOP. This study aimed to address the quantitative assessment of these features in a cohort of patients with FOP, which potentially helps early diagnosis of FOP. Radiographs of the hand and cervical spine were retrospectively analyzed from a total of 18 FOP patients (9 males and 9 females) with an average age of 13.9 years (range 0.7-39.3 years). The elevated ratio of the second metacarpal bone to the distal phalanx of the thumb (> +1SD) was a consistent finding irrespective of the patient's age and gender. Infant FOP patients, in addition, exhibited an extremely high ratio of the second metacarpal bone to the first metacarpal bone (> +3SD). The height/depth ratio of the C5 vertebra increased in patients over 4 years of age (> +2SD). Additionally, the ratio of (height+depth) of the C5 spinous process to the C5 vertebral depth was markedly elevated in young patients (> +2SD). We quantitatively demonstrated the hand and cervical spine characteristics of FOP. These findings, which can be seen from early infancy, could be useful for early diagnosis of FOP even in patients without great toe abnormalities.**

Keywords: Fibrodysplasia ossificans progressiva, early diagnosis, radiographic characteristics

1. Introduction

Fibrodysplasia ossificans progressiva (FOP) is a severely disabling genetic disorder of connective tissues characterized by congenital malformations of the great toes and progressive heterotopic ossification (HO) in various extraskeletal sites including muscles, tendons, ligaments, fascias, and aponeuroses. FOP is caused by a recurrent activating mutation (c.617G > A, p.R206H) in the gene encoding activin receptor IA/activin-like kinase 2 (ACVR1/ALK2), a bone morphogenetic protein (BMP) type I receptor (*1*). HO typically begins to form during the first decade of life preceded by painful soft tissue swelling and inflammation (flare-ups), which are sometimes mistaken for aggressive fibromatosis or musculoskeletal tumors. Surgical resection of HO leads to explosive new bone formation (*2*). Since there is no definitive treatment to prevent progressive HO in FOP to date (*3*), early correct diagnosis is necessary to maintain their mobility by preventing additional iatrogenic harm (*4*).

Malformations of the great toes, such as hallux valgus, deformed proximal phalanges and shortened first metatarsal bones, are well-known pre-osseous features of FOP (*5*). A reported incidence of these deformities is 95%, suggesting that there exists rare FOP cases without the great toe abnormalities (*6*). We demonstrated additional early radiographic signs of FOP including shortening of the first metacarpal bones and hypertrophy of the posterior element of the cervical

*Address correspondence to:
Dr. Hiroshi Kitoh, Department of Orthopaedic Surgery, Nagoya University Graduate School of Medicine, 65 Tsurumai, Showa-ku, Nagoya, Aichi, 466-8550, Japan.
E-mail: hkitoh@med.nagoya-u.ac.jp

spine (*7*). Clinical awareness of these deformities can aid clinicians in making early diagnosis of FOP, but quantitative assessment of these deformities has not yet been determined.

In this study, we retrospectively examined radiographs of the hand and cervical spine in FOP patients and demonstrated various abnormal radiographic parameters helpful for early diagnosis of this specific disorder.

2. Materials and Methods

2.1. *Demographics*

This study represents a retrospective case-control study consisting of Japanese FOP patients followed up at health care facilities where members of the Research Committee on Japanese Fibrodysplasia Ossificans Progressiva practiced. After approval from the Institutional Review Board of the Nagoya University Hospital, we collected the hand and/or cervical spine radiographs from 18 FOP patients (9 males and 9 females) with an average age of 13.9 years (range 0.7-39.3 years) at the time of this study. The patients were diagnosed clinically and radiographically based on various characteristic findings of FOP including deformities of the great toes, extraskeletal HO, joint contractures, cervical fusions, broad femoral necks, and osteochondroma-like lesions. Molecular testing was performed on fourteen patients. Thirteen showed the common *ACVR1/ALK2* mutation within the glycine/serine-rich regulatory (GS) domain (c.617G > A, p.R206H), and one patient had an atypical mutation within the protein kinase domain (c.774G > T, p.R258S). Molecular studies were not conducted for the remaining 4 patients who showed characteristic skeletal features of FOP. We examined anteroposterior (AP) radiographs of the hands and lateral radiographs of the cervical spine in each individual. The earliest hands and cervical spine films were analyzed using image processing and analysis software ImageJ®.

2.2. *Radiographic assessment of the hand*

According to the measurement method by Poznanski *et al.* (*8*), the length of each phalanx and metacarpal bone was measured. In brief, the tangent lines were drawn at both ends of each bone, which were perpendicular to the bone axis, and a bone length was defined as the distance between these two lines (Figure 1). We measured a length of the distal (D1) and proximal (P1) phalanges of the thumb as well as that of the first and second metacarpal bones (MET1 and MET2), and calculated the following bone length ratios, MET2/MET1, MET2/P1, MET2/D1, MET1/P1, MET1/D1, and P1/D1. Radiographs of both hands from one patient were separately analyzed to obtain the average value of the measurements. Reference ranges of these measurements in different ages and genders were used based on the literature from Poznanski *et al.* (*8*). The control data of these measurements in infant (n = 21) were determined by the radiographic database in Nagoya University Hospital.

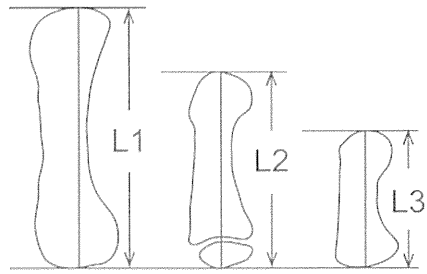

Figure 1. A schematic diagram illustrating the measurement method of bone length in the hand. Bone length was defined as the distance between the tangents drawn to each end of the bone, which were perpendicular to the bone axis. The entire bone length was measured for adults (L1), children (L2), and infants (L3).

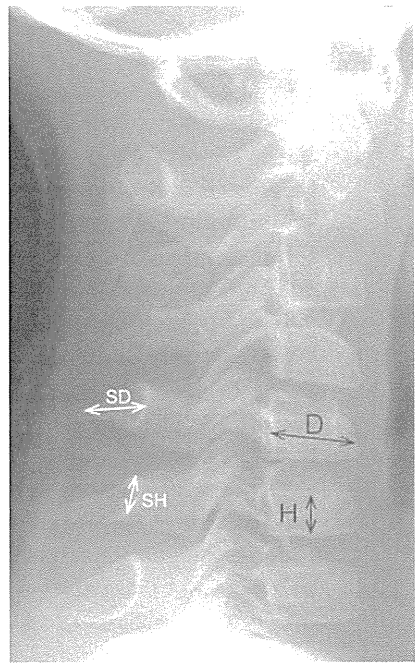

Figure 2. A radiograph depicting the measurements of the bone length in the cervical spine. The height (H) and depth (D) of the C5 vertebral body was measured at the midportion of the body. The height of the C5 spinous process (SH) was defined as the distance from the cranial to the caudal rim at the juxta-laminar zone. The depth of the spinous process (SD) was measured from the midpoint of the anterior wall to that of the posterior rim.

2.3. *Radiographic assessment of the cervical spine*

According to the measurement method proposed by Remes *et al.* (*9*), the height and depth of the C5 vertebral body were measured. Briefly, vertebral body height (H) was measured at the midpoint of the vertebra, perpendicular to the lower end plate. The vertebral body depth (D) was measured at the midpoint of the body from the anterior wall to the posterior wall (Figure 2). The H/D ratios of the C5 vertebra were then calculated

Table 1. Characteristics and quantitative indices for the study population

Patient	Sex	ALK2 mutation	Age at X-ray (yrs)	Deviation of the bone length ratios (SD)			
			Hand/Cervical spine	MET2/D1	MET2/D1	H/D	(SH+SD)/D
1	M	R206H	0/0	1.0	1.0	0.6	0.1
2	M	R206H	0/0	2.4	2.4	0.6	7.1
3	M	R206H	1/3	3.1	3.1	0.9	2.8
4	F	R206H	5/6	2.8	2.8	3.3	8.3
5	M	R206H	8/7	6.2	6.2	2.8	3.7
6	M	R206H	12/18	4.1	4.1	1.9	1.5
7	F	R206H	17/17	4.0	4.0	4.1	NA
8	F	R206H	20/NA	2.2	2.2	NA	NA
9	M	R206H	29/NA	2.7	2.7	NA	NA
10	M	R206H	34/NA	3.5	3.5	NA	NA
11	F	R206H	36/NA	1.0	1.0	NA	NA
12	M	R206H	39/16	1.9	1.9	3.0	1.8
13	F	R206H	NA/18	NA	NA	0.6	2.4
14	F	R258S	14/14	1.7	1.7	4.9	NA
15	M	ND	NA/4	NA	NA	3.2	8.8
16	F	ND	NA/8	NA	NA	9.2	7.9
17	F	ND	NA/16	NA	NA	4.4	NA
18	F	ND	5/5	5.3	5.3	5.3	5.4

M denotes male; F, female; ND, not determined; NA, not applicable; SD, standard deviation.

and compared to normal reference values established by Remes *et al.* in different age and gender groups (*9*). In addition, we measured the height and depth of the C5 spinous process. The height of the spinous process (SH) was defined as the distance from the cranial to caudal margin at the junction of the spinous process and lamina. The depth of spinous process (SD) was measured from the midportion of the anterior wall to that of the posterior rim demarcating a thick cortex shadow (Figure 2). The sum of SH and SD measurements was used for the evaluation of spinous process size, then the (SH + SD)/D ratio of the C5 vertebra was calculated. Reference values of the (SH + SD)/D ratio were established from the radiographic database of normal controls in Nagoya University Hospital.

3. Results

3.1. *Characteristics of the study cohort*

Patients' characteristics and quantitative indices of the measurements are shown in Table 1. Deviation of the bone length ratios in the hand and cervical spine was calculated based on age-matched reference values.

3.2. *Radiographic characteristics of the hand*

Mean and standard deviation of the MET2/D1 and MET2/MET1 ratio in control infants (n = 21) are 2.9 ± 0.29 and 1.64 ± 0.08, respectively. Twenty-six hand radiographs from 14 patients (8 males and 6 females) were available. Regardless of age and gender, all FOP patients showed a MET2/D1 ratio larger than +1SD of normal controls (Figure 3A and 3B). In infant patients without an epiphyseal ossification center of the first metacarpal bone, the MET2/MET1 ratio was extremely

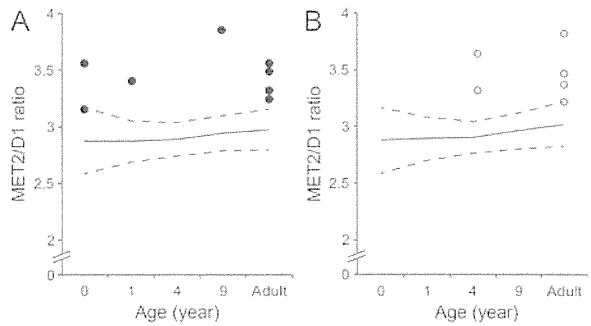

Figure 3. Scatter plots showing the bone length ratio of the second metacarpal bone (MET2) to the distal phalanx of the thumb (D1) in male (A) and female (B) patients with FOP. Solid and dash lines denote the normal value and the standard deviation (SD) of the MET2/D1 ratio, respectively.

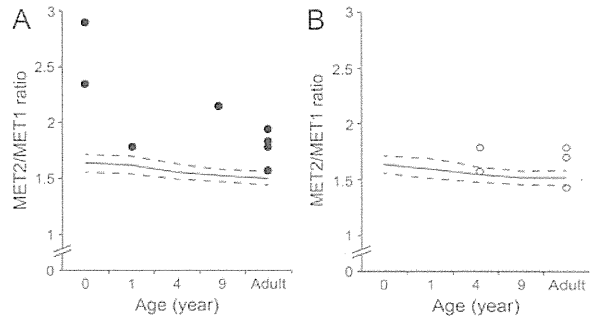

Figure 4. Scatter plots showing the bone length ratio of the second metacarpal bone (MET2) to the first metacarpal bone (MET1) in male (A) and female (B) patients with FOP. Solid and dash lines denote the normal value and the standard deviation (SD) of the MET2/MET1 ratio, respectively.

large (> +3SD of normal controls) (Figure 4A and 4B). The MET2/P1 ratio was higher in infant patients, but it scattered around the mean value with increasing age (data not shown). There were no characteristic features in the values of the MET1/P1, MET1/D1, and P1/D1 ratios in FOP patients, although the MET1/P1 and MET1/D1

Table 2. Mean and standard deviation of normal controls for the (SH+SD)/D ratio of the C5 vertebra

Age group	<1	1-2	2-3	3-4	4-5	5-6	6-7	7-8	8-9	9-10	10-11	11-12	12-13	13-14	14-15	15-16	16-17	17-18	18-19	19-20	20-21
Mean	1.05	1.10	1.09	1.20	1.21	1.43	1.37	1.47	1.33	1.47	1.50	1.53	1.51	1.57	1.69	1.86	1.76	1.73	1.71	1.78	1.86
SD	0.13	0.15	0.15	0.13	0.11	0.18	0.18	0.17	0.19	0.18	0.16	0.18	0.20	0.19	0.12	0.16	0.22	0.22	0.23	0.24	0.25
N	11	21	17	13	6	13	25	19	20	17	16	17	14	20	16	21	23	31	28	38	20

SD denotes standard deviation; N, number of control subjects; SH, height of the spinous process; SD, depth of the spinous process; D, depth of the vertebral body.

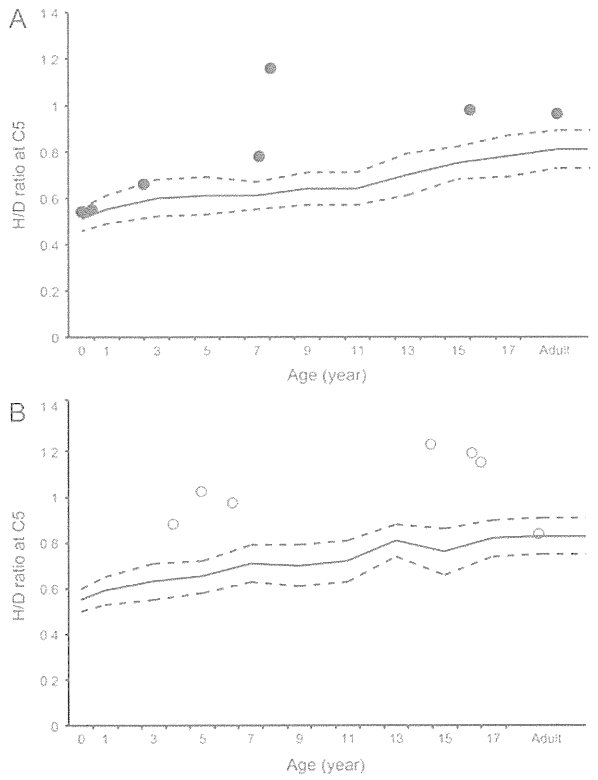

Figure 5. Scatter plots showing the bone length ratio of the C5 vertebral height (H) to depth (D) in male (A) and female (B) patients with FOP. Solid and dashed lines denote the normal value and the standard deviation (SD) of the H/D ratio, respectively.

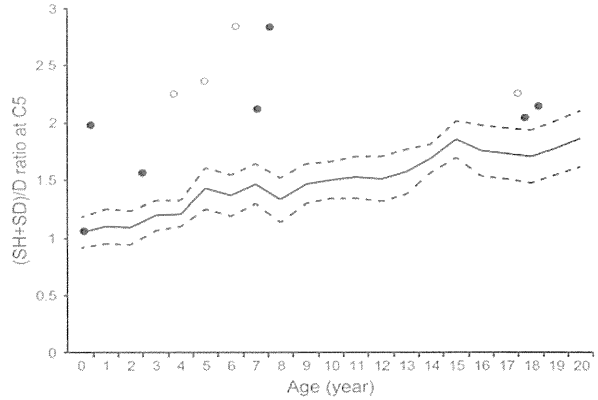

Figure 6. Scatter plots showing the bone length ratio of the C5 spinous process height (SH) + depth (SD) to the C5 vertebral depth (D). Solid and open circles indicate male and female, respectively. Solid and dashed lines denote the normal value and the standard deviation (SD) of the (SH+SD)/D ratio, respectively.

ratios were relatively small (< -1SD of normal controls) in infant FOP patients (data not shown).

3.3. *Radiographic characteristics of the cervical spine*

Reference values of the (SH + SD)/D ratio of the C5 vertebra are shown in Table 2. There were 14 (7 males and 7 females) cervical spine radiographs available for analysis. Among them, three radiographs were excluded from analysis of the (SH + SD)/D ratio for insufficient resolution. The H/D ratio of the C5 vertebra exceeded +2SD of normal controls in patients over 4 years of age except one female adult patient (Figure 5A and 5B). Similarly, the (SH + SD)/D ratio of the C5 vertebra was larger than +2SD of normal controls in young patients except one male infant (Figure 6).

4. Discussion

In the present study, we quantitatively proved the hand and cervical spine abnormalities in FOP including shortened thumbs as well as tall and narrow vertebral bodies and hypertrophic posterior elements of the cervical spine (*7,10*). Especially in young patients, shortening of the first metacarpal bone and enlargement of the cervical spinous processes were pathognomonic findings useful for early diagnosis of FOP before the appearance of HO.

Previous studies have reported that thumb shortening was seen in 50% of FOP patients (*6*). In the present study, all patients had a MET2/D1 ratio larger than +1SD of normal controls, and 85% (11/13) of the patients showed an increased MET2/MET1 ratio. The thumb shortening, therefore, seems to be more common than previous reports in FOP. Furthermore, an extremely high MET2/MET1 ratio in infant patients suggested that disproportionate shortening of the first metacarpal bone was an important early radiographic finding in FOP (Figure 7).

It is an intriguing feature of FOP that thumb morphogenesis is exclusively disrupted in the development of digit formation (*11*). The thumb is the last digit in the autopod to form, and it is different from other digits in terms of its relative position, shape, size, and number of phalanges. These unique thumb identities may be attributed to the expression profile of *HoxD* genes, which are pivotal transcriptional factors regulating limb patterning and growth (*12*). All four *HoxD10* to *D13* genes are expressed in the future digit II-V area in the autopod during the hand plate formation, whereas sole expression of the